

# A Frequency Control Method for Regulating Wireless Power to Implantable Devices

Ping Si, *Member, IEEE*, Aiguo Patrick Hu, *Senior Member, IEEE*, Simon Malpas, and David Budgett

**Abstract**—This paper presents a method to regulate the power transferred over a wireless link by adjusting the resonant operating frequency of the primary converter. A significant advantage of this method is that effective power regulation is maintained under variations in load, coupling and circuit parameters. This is particularly important when the wireless supply is used to power implanted medical devices where substantial coupling variations between internal and external systems is expected. The operating frequency is changed dynamically by altering the effective tuning capacitance through soft switched phase control. A thorough analysis of the proposed system has been undertaken, and experimental results verify its functionality.

**Index Terms**—Frequency control, inductive power transfer, wireless power (WP).

## I. INTRODUCTION

IMPLANTABLE biomedical devices have found applications in a wide range of areas, including pacemakers, cochlear implants, physiological monitoring devices, drug infusion devices, functional electrical stimulators (FES), left ventricular assist devices (LVAD), and artificial hearts. The traditional approach to supplying power to these devices is implantable batteries and percutaneous links [1]–[3]. However, any battery has a limited energy storage and life span, and percutaneous links are susceptible to infection and reliability problems. Wireless power (WP) supplies offer the opportunity to provide power for indefinite periods without the risk of infection from a percutaneous lead.

A WP supply making use of magnetic fields for energy transfer will consist of a primary (external) power circuit and a secondary implantable power pick-up. A primary converter employed in the primary station produces a high frequency alternating current flowing through an external coil (track), generating an alternating electromagnetic field. The presence of the time varying field within the secondary coil induces currents which can be converted to power an implanted device.

A common characteristic associated with biomedical applications is loose coupling between the primary and secondary coils. Compensation for loose coupling can be achieved through the use of resonance circuits which enables the voltage (or current)

Manuscript received June 28, 2007; revised January 14, 2008. This work was supported in part by School of Engineering Guaranteed Financial Support Scheme (GFSS), The University of Auckland, and Telemetry Research Limited, New Zealand. This paper was recommended by Associate Editor J. Chen.

P. Si and A. P. Hu are with the Department of Electrical and Computer Engineering, The University of Auckland, Auckland 1142, New Zealand (e-mail: psi001@ec.auckland.ac.nz; a.hu@auckland.ac.nz).

S. Malpas and D. Budgett are with the Bioengineering Institute, The University of Auckland, Auckland 1142, New Zealand (e-mail: s.malpas@telemetryresearch.ac.nz; d.budgett@auckland.ac.nz).

Digital Object Identifier 10.1109/TBCAS.2008.918284

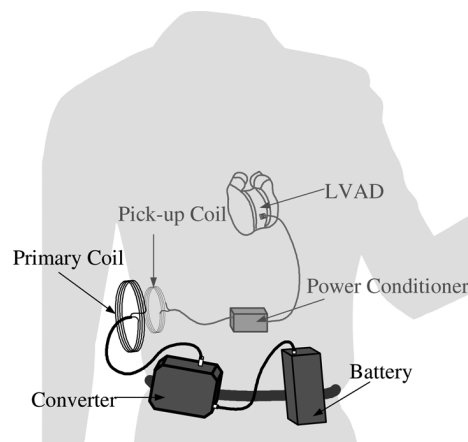


Fig. 1. High-power closely coupled WP supply.

at the secondary to boost up to useful levels even in the presence of low coupling coefficients. The ability to achieve power transfer is dependent on the match between the resonant frequency of the primary with the resonant frequency of the secondary. In applications such as cochlear implants the external coil can be fitted to the skin on the scale in a consistent manner and the coupling coefficient is repeatable. However, for high power applications, such as LVADs, the size of WP systems dictate that they must be located in soft tissue locations where the coupling conditions are likely to vary not only between patients, but from day-to-day activities such as posture changes and fitting. Although some efforts have been made to provide consistent coupling, these can lead to skin irritation and lesions. This work presents a method of regulating power which is robust to variations in coupling.

Power regulation can be achieved at the implantable pick-up side [4], [5]. However, the energy dissipation associated at the implant may lead to increased temperature of tissue surrounding the implantable device. This can be significant even when the overall power efficiencies are at the level of 90% [6]. Power regulation circuits also require extra physical components which increase the size and weight of the devices. To minimize the size and power losses, methods to control power flow directly from primary power circuits have been developed [6]–[10], among which voltage magnitude regulation at the primary power converter is the most popular. If a WP supply is guaranteed to operate at or close to the full tuning condition of the system, the magnitude regulation method can be efficient. However, in practice the resonant frequency of the secondary pick-up circuit is often mismatched with the operating frequency of the primary because of the variations in load, coupling and other circuit parameters. When mismatching occurs, the voltage magnitude

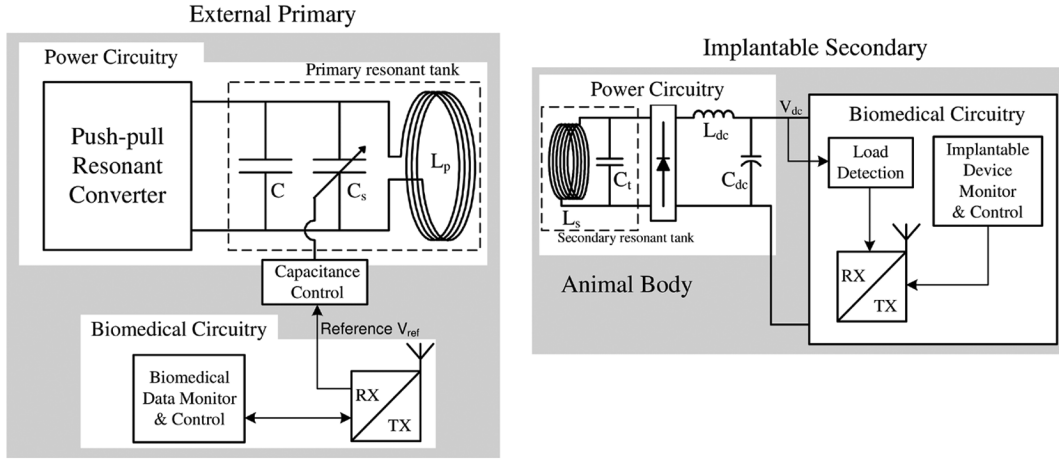


Fig. 2. System configuration of proposed WP supply capacity, EMI, tissue heating, and ZVS operation.

control approach can only respond by operating at a high magnitude to attempt to maintain the power flow to the load.

In this paper, a frequency control method is proposed for regulating the operating frequency of the WP supply. Regulating the frequency can tune/detune the secondary power pick-up according to the actual load requirements. When the full tuning condition is changed due to the parameter variations, the frequency control method can be used to track the new tuning condition.

A switched-capacitor method of varying the effective resonant capacitance of the primary power converter is proposed and developed. This method offers dynamic control of the operating frequency of the WP supply while retaining low switching losses and smooth frequency variations.

## II. WP SUPPLY ARCHITECTURE

High power implantable devices such as LVADs and artificial hearts require up to 10–30 W of power. Fig. 1 illustrates a typical WP supply configuration for a LVAD. The primary coil is placed outside of a patient, driven by a converter power from a portable battery. The secondary power pick-up coil is implanted under the skin, facing the primary coil. Typically the coupling coefficient of such a system will be within the range of 0.1–0.3, and the distance between the external and internal coils is less than 3 cm [11].

Fig. 2 illustrates the system structure of a WP supply with frequency control at the primary converter. A current-fed push–pull resonant converter is employed at the primary side due to its advantages of high efficiency, low harmonics and small physical size [12]. In Fig. 2, the primary track (coil) is represented by an inductor  $L_p$ , which connects to a constant capacitor  $C$  and a variable capacitor  $C_s$  in parallel, forming a resonant tank. The operating frequency of the WP supply is equal to the push–pull converter zero-voltage-switching (ZVS) frequency given in (1), which can be derived from the analytical analysis in [13]

$$\omega = \frac{\left( \sqrt{\frac{(1 - \frac{1}{4Q^2})}{(L_p(C + C_s))}} - \frac{\varphi}{T} \right)}{\left( 1 + \frac{2\varphi}{\pi} \right)} \quad (1)$$

where  $\varphi$ ,  $Q$ , and  $T$  are the initial phase angle, the quality factor, and the time constant of the resonant tank. It can be seen from (1) that the operating frequency is dependent on the capacitance  $C_s$ .

The secondary pick-up coil is represented by  $L_s$  in Fig. 2.  $L_s$  is parallel tuned with capacitor  $C_t$ . The voltage induced in the pick-up coil can be boosted up according to the designed boost-up-factor of the resonant circuit [14]. Using air core windings for the primary and secondary coils reduces weight and temperature rise by eliminating core losses. The dc inductor  $L_{dc}$  is to maintain the continuous current flow through the rectifier, making power transfer from ac to dc side smooth and uninterrupted [14].

It is complicated to determine an optimal operating frequency of a WP supply, because there are many factors that need to be considered—including physical size, power efficiency, power capacity, electromagnetic interference (EMI), tissue heating, and ZVS operation.

The physical size and the ZVS operating conditions are the key factors that limit the minimum operating frequency [13]. The power transfer capacity and EMI limit the maximum frequency [15]. The power efficiency can feature at both the low and high boundaries of the operating frequency [16]. Our experience suggests a frequency between 50 and 500 kHz is suitable for a WP supply. Although a higher operating frequency can reduce the physical size of circuit, the power efficiency would decrease due to the increase in switching losses.

## III. ANALYSIS OF POWER FLOW AGAINST FREQUENCY

To design a WP supply based on frequency control, it is necessary to analyze the relationship between the power follow and the operating frequency of the system. It is also necessary to determine the range in frequencies required to allow for load, coupling and circuit parameter variations.

Fig. 3 shows the Thevenin equivalent of a parallel tuned pick-up circuit used in the secondary side of the WP supply. The ac voltage source  $v_{oc}$  represents the open circuit voltage induced in the pick-up coil. The output dc voltage  $V_{dc}$  is supplied to the load. For maximum power transfer purpose, the dc inductance  $L_{dc}$  is normally designed to be larger than a value

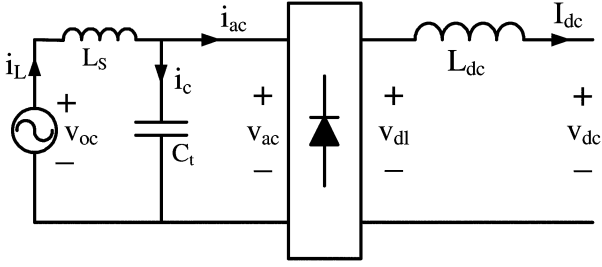


Fig. 3. Thevenin equivalent of a parallel tuned pick-up circuit.

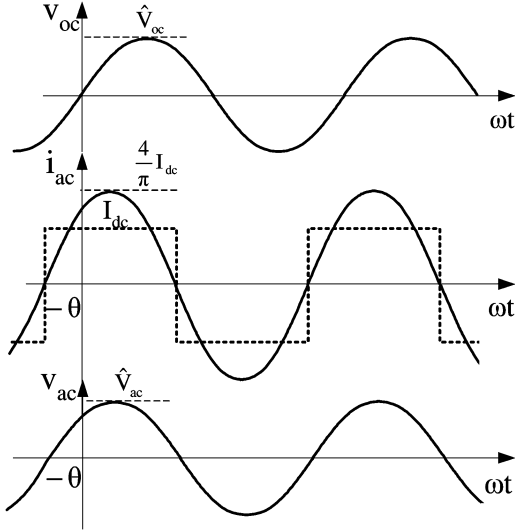


Fig. 4. Current and voltage waveforms of the pick-up.

determined by (2) to ensure the continuation of the dc current  $I_{dc}$  under the steady-state conditions [14]. This also means that the input current of the rectifier  $i_{ac}$  is in the shape of a square waveform having an approximate constant magnitude of  $I_{dc}$

$$L_{dc} = \frac{R_{min}}{\omega} \quad (2)$$

where  $R_{min}$  is the equivalent resistance of the maximum load.

Fig. 4 shows the steady-state current and voltage waveforms as seen by the inductor in the pick-up. Neglecting harmonics, the current  $i_{ac}$  appears as a sinusoidal waveform with the peak value of  $4I_{dc}/\pi$ , being the amplitude of the fundamental component of the Fourier series. The current  $i_{ac}$  and voltage  $v_{ac}$  are in phase because the diodes of the rectifier conduct only when forward voltages are applied. Specifying the phase angle difference between voltage  $v_{ac}$  and  $v_{oc}$  to be  $\theta$ , as shown in Fig. 4, the phasor of the current  $i_{ac}$  can be determined by (3). In addition, the amplitude of  $v_{ac}$  is governed by the output dc voltage  $V_{dc}$  according to (4). This indicates that the voltage  $v_{ac}$  will remain constant as the pick-up output voltage is maintained constant at  $V_{dc}$

$$\dot{I}_{ac} = \frac{4}{\pi} I_{dc} \angle \theta \quad (3)$$

$$\hat{V} = \frac{\pi V_{dc}}{2}. \quad (4)$$

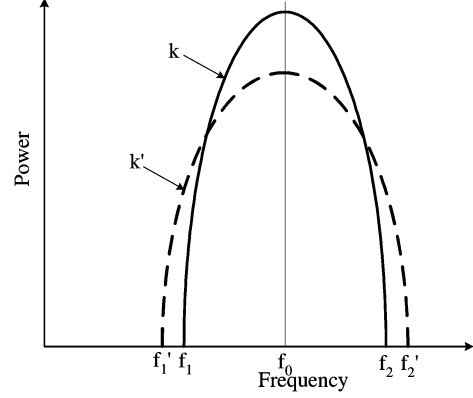


Fig. 5. Relationship between power and frequency.

Under steady-state conditions, the following equation can be obtained using the relationship  $\dot{I}_{ac} = \dot{I}_L - \dot{I}_c$ :

$$\begin{aligned} & \frac{4}{\pi} I_{dc} \cos(\theta) + j \frac{4}{\pi} I_{dc} \sin(\theta) \\ &= \hat{V}_{ac} \sin(\theta) \left( \omega C_t - \frac{1}{\omega L_s} \right) \\ &+ j \left[ \hat{V}_{ac} \cos(\theta) \left( \frac{1}{\omega L_s} - \omega C_t \right) - \frac{\hat{V}_{oc}}{\omega L_s} \right] \end{aligned} \quad (5)$$

where  $\hat{V}_{oc}$  is the amplitude of  $v_{oc}$ .

The average power induced in the pick-up coil is determined by

$$P = \text{Re}(\dot{V} \dot{I}_L^*) = \frac{\hat{V}_{ac} \hat{V}_{oc} \sin(\theta)}{\omega L_s}. \quad (6)$$

Since the induced power in the pick-up cannot be negative, the phase angle  $\theta$  must be between  $\pi$  and  $2\pi$ . Therefore, based on (5) and (6),  $P$  and  $\theta$  can be expressed as

$$\begin{aligned} P &= I_{dc} V_{dc} \\ &= \frac{k\pi \hat{V}_{oc}^2}{4\sqrt{2}} \sqrt{\left( \frac{1}{\omega L_s} \right) - \left[ \frac{k\pi}{2\sqrt{2}} \left( \omega C_t - \frac{1}{\omega L_s} \right) \right]^2} \end{aligned} \quad (7)$$

$$\cos(\theta) = \frac{k\pi}{2\sqrt{2}} \cdot \frac{(\omega C_t - 1/(\omega L_s))}{1/(\omega L_s)} \quad \pi < \theta < 2\pi \quad (8)$$

where  $k$  is the boost-up-factor defined by (9) [14]

$$k = \frac{\sqrt{2} V_{dc}}{\hat{V}_{oc}} = \frac{2\sqrt{2} \hat{V}_{ac}}{\pi \hat{V}_{oc}}. \quad (9)$$

According to (7), the power  $P$  will vary with frequency  $\omega$ . This shows the basis for using the control of frequency to achieve regulation of power. In addition, it can be seen that controlling the primary frequency can also compensate for the errors and variations of the circuit parameters including  $k$ ,  $C_t$ ,  $L_s$ , and  $v_{oc}$ .

Fig. 5 illustrates the steady-state relationship between the power flow  $P$  and the operating frequency  $f$ . It can be seen that the shape of the relationship between  $p$  and  $f$  is parabolic with a maximum occurring at the natural resonant frequency

$f_0$ . This frequency is the full tuning frequency of the pick-up, whose value is determined by  $\omega_0 = 1/\sqrt{L_s C_t}$ . The maximum

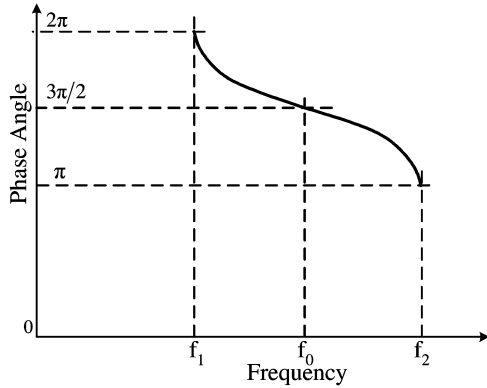


Fig. 6. Relationship between phase angle and frequency.

power can be calculated using (7) with the angular frequency  $\omega_0$ . The result is  $1.11V_{oc}V_{dc}/(\omega_0 L_s)$  which is consistent with the analytical result obtained in [14]. Zero power is transferred when the WP supply operates at the boundary frequency  $f_1$  and  $f_2$ .

As a comparison, the power transfer for a reduced value of boost-up-factor  $k'$  is also shown in Fig. 5. The maximum power for the boost-up-factor  $k'$  is obtained at the same full tuning frequency  $f_0$ , but the magnitude of the peak is less. However, the curve for  $k'$  has a wider frequency range, from  $f'_1$  to  $f'_2$  shown in Fig. 5. This indicates that the WP supply with a higher boost-up-factor needs more accurate frequency control with a higher resolution to achieve equivalent power regulation than a system with a lower boost-up-factor.

Fig. 6 shows the relationship between the phase angle  $\theta$  and the operating frequency  $f$ . It can be seen that the phase angle  $\theta$  moves from  $2\pi$  to  $\pi$  while the frequency  $f$  varies from the boundary  $f_1$  to  $f_2$ . Actually, the phase angle is the power transfer angle of the pick-up. If  $k$  is constant, varying the frequency changes the power transfer angle, so that the power delivered in the pick-up is changed. According to (8), when the system operates at the full tuning frequency  $\omega_0$  for maximum power transfer, the phase angle  $\theta$  is equal to  $3\pi/2$ .

The boundary frequency  $f_1$  and  $f_2$  are the minimum and maximum frequencies for maintaining the constant output dc voltage  $V_{dc}$ . These are valid and valuable operating frequencies for some application where the load may have almost no power demands while in a standby mode. Under the zero load conditions, if the WP supply can not operate at these boundary frequencies, the output dc voltage  $V_{dc}$  would be under or over the nominal value required by biomedical devices. For example, a biomedical device may go into sleep mode so that no power or very little power is required. This situation can be considered as the zero load condition. If the system operates at a frequency which is between  $f_1$  and  $f_2$ , too much power would be delivered to the pick-up causing a higher voltage output which may damage the biomedical device. Conversely, if the system operates at a frequency which is either under  $f_1$  or over  $f_2$ , the output dc voltage of the pick-up would be under the nominal value so that the biomedical device may not work properly.

When zero current is supplied to the load, the amplitude of the resonant voltage  $v_{ac}$  must be equal to the output dc voltage  $V_{dc}$ , as shown in (10)

$$|\hat{V}_{ac}| = \left| \frac{\hat{V}_{oc} \angle 0}{j\omega L_s + \frac{1}{(j\omega C_t)} \cdot \frac{1}{j\omega C_t}} \right| = \left| \frac{\hat{V}}{1 - \omega^2 L_s C_t} \right| = V_{dc} \quad (10)$$

and the values of  $f_1$  and  $f_2$  are found to be

$$f_{1,2} = \frac{1}{2\pi} \sqrt{\frac{V_{dc} \pm \hat{V}_{oc}}{V_{dc} L_s C_t}} \quad (11)$$

#### IV. SWITCHED CAPACITOR FREQUENCY CONTROL METHOD

As discussed earlier, the primary frequency can be varied by changing the effective capacitance of the primary resonant tank.

A direct on-off control of a capacitor bank has been developed for changing resonant capacitance. A number of capacitors are placed at the input port of the resonant tank, and they are controlled to be in and out by direct hard switching of semiconductor devices such as MOSFETs [17]. Because changing the capacitance is implemented by hard switching in one of a number of capacitors in discrete steps, the frequency can not be smoothly varied. Moreover, the hard switching of the capacitors can cause larger switching losses, and resultant surge currents can damage the switching devices. The step size can be reduced and the frequency variation range can be increased by having more capacitors and switching devices, but the system size, cost and reliability would be compromised.

To reduce the power losses and achieve smooth variations of the frequency, a new method to change the resonant capacitance is proposed and implemented. A variable capacitance is controlled by soft switching a capacitor with a varied duty cycle. This means that the effective capacitance of a capacitor is controlled by changing the average charging and discharging period of the capacitor. Because soft switching can be achieved, there is no destructive surge current to damage the switching devices. A frequency variation range is only determined by the total capacitance rather than the number of capacitors.

Fig. 7(a) shows the basic structure of the push-pull resonant converter with the implementation of the frequency control. Inductor  $L$  (primary coil or track), fixed tuning capacitor  $C$ , and switched capacitors  $C_{s1}$  and  $C_{s2}$  form the primary resonant tank. The main switches  $S_1$  and  $S_2$  are switched on and off alternatively for half a resonant period. When the converter shown in Fig. 7(a) operates in the duration when  $S_1$  is on and  $S_2$  is off, its equivalent circuit is shown in Fig. 7(b). Capacitor  $C_{s1}$  is not involved due to grounding through the main switch  $S_1$ . Similarly, the capacitor  $C_{s2}$  will not be involved in the resonant tank when the converter operates in the duration when  $S_2$  is on and  $S_1$  is off.

Soft switching is important to ensure that destructive surge currents are not generated when switching the capacitor. This is achieved using the phase control method shown in Fig. 8.  $v_{syn}$  is the signal of the resonant voltage  $v_c$ .  $V_{ref}$  is a reference dc voltage. Gate control signals  $v_{gsw1}$  and  $v_{gsw2}$  for  $S_{w1}$  and  $S_{w2}$  are generated by comparing  $V_{ref}$  to  $v_{syn}$  and  $-v_{syn}$ . Setting the

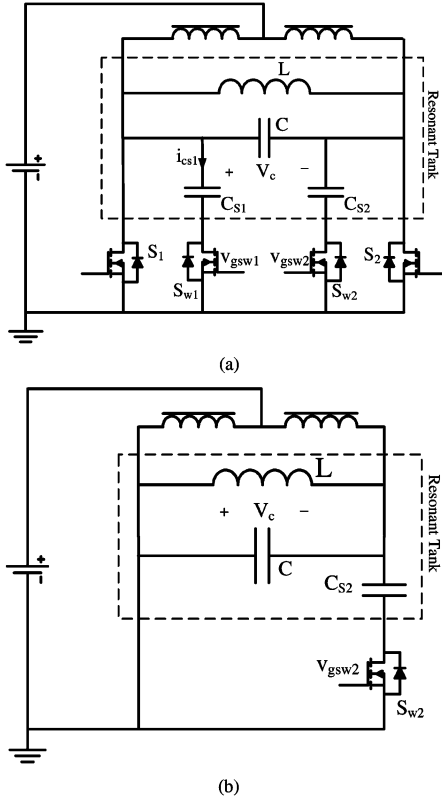


Fig. 7. Current-fed push-pull resonant converter with variable frequency and its equivalent circuit. (a). Basic topology of variable frequency push-pull resonant converter. (b). Equivalent circuit of converter when switch  $S_1$  on and  $S_2$  off.

voltage  $V_{ref}$  determines the duty cycle of the gate control signals. In a WP supply,  $V_{ref}$  is a feedback signal from the secondary side representing the actual power demand of the load. Fig. 9 shows the waveforms of  $v_{syn}$ ,  $V_{ref}$ ,  $v_{gsw1}$ , and current  $i_{cs1}$  flowing through the switched capacitor  $C_{s1}$ . The switching angle  $\alpha$  and duty cycle of the gate control signal  $v_{gsw1}$  are varied in response to changes of  $V_{ref}$ . At the beginning of switching on, the current  $i_{cs1}$  is seen to be negative. This means the current is flowing through the body diode of the switch  $S_{w1}$ . Neglecting the voltage drop of the diode, zero voltage switching is achieved.

If the capacitances of  $C_{s1}$  and  $C_{s2}$  are equal, the net effect of switching  $C_{s1}$  and  $C_{s2}$  over a resonant period is equivalent to that of switching one capacitor of value  $C_{s1}$  using dual side switching [12]. Therefore, the effective capacitance is determined by (12)

$$C_s = \frac{2C_{s1}[1 - \cos(\alpha)] + C_{s1}(\pi - 2\alpha)\sin(\alpha)}{2}. \quad (12)$$

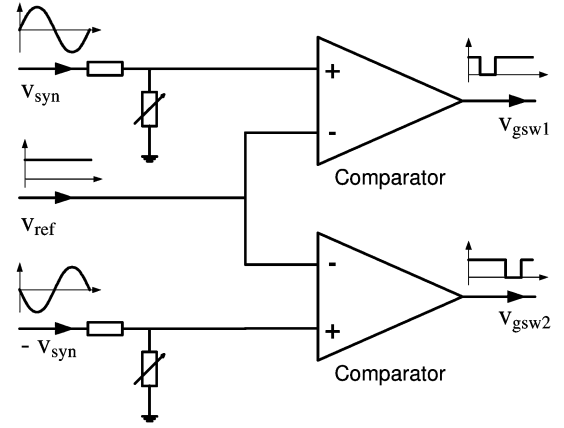


Fig. 8. Structure of phase control.

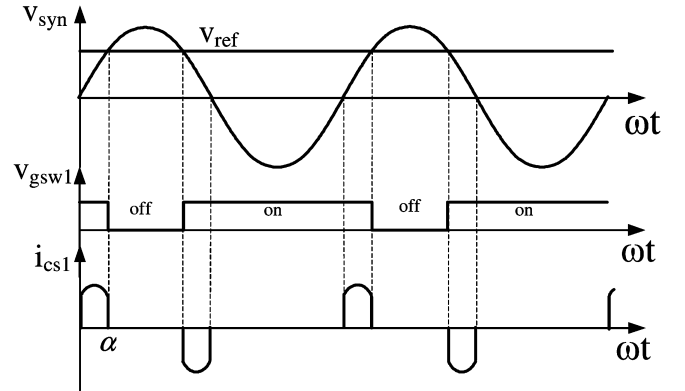


Fig. 9. Waveforms of push-pull resonant converter with switched capacitors.

The effective capacitance  $C_s$  can vary from zero to  $C_{s1}$  when switching angle  $\alpha$  varies from  $0^\circ$  to  $90^\circ$ .

The switching angle  $\alpha$  is determined by

$$\alpha = \arcsin\left(\frac{V_{ref}}{\hat{V}_{syn}}\right) \quad (13)$$

where  $\hat{V}_{syn}$  is the amplitude of the signal  $v_{syn}$ .

According to (1), (12), and (13), it can be shown that the operating frequency  $\omega$  is a function of  $V_{ref}$ , shown in (14) at the bottom of the page.

Then, depending on (7), a closed form relationship between  $V_{ref}$  and power  $P$  can be determined by (15) at the bottom of the next page.

In practice, load changes would instantly cause variations in the secondary output voltage  $V_{dc}$ . Therefore, the changes in the power demand can be detected by monitoring the variation of

$$\omega = f(V_{ref}) = \frac{T\sqrt{\left(1 - \frac{1}{4Q^2}\right) - \varphi} \sqrt{L_p \left( C + C_{s1} \left[ 1 - \sqrt{1 - \left(\frac{V_{ref}}{\hat{V}_{syn}}\right)^2} \right] + \frac{C_{s1}}{2} \left( \pi - 2 \arcsin\left(\frac{V_{ref}}{\hat{V}_{syn}}\right) \right) \left(\frac{V_{ref}}{V_{ref}}\right) \right)}}{T\left(1 + \frac{\varphi}{\pi}\right) \sqrt{L_p \left( C + C_{s1} \left[ 1 - \sqrt{1 - \left(\frac{V_{ref}}{\hat{V}_{syn}}\right)^2} \right] + \frac{C_{s1}}{2} \left( \pi - 2 \arcsin\left(\frac{V_{ref}}{\hat{V}_{syn}}\right) \right) \left(\frac{V_{ref}}{V_{ref}}\right) \right)}} \quad (14)$$

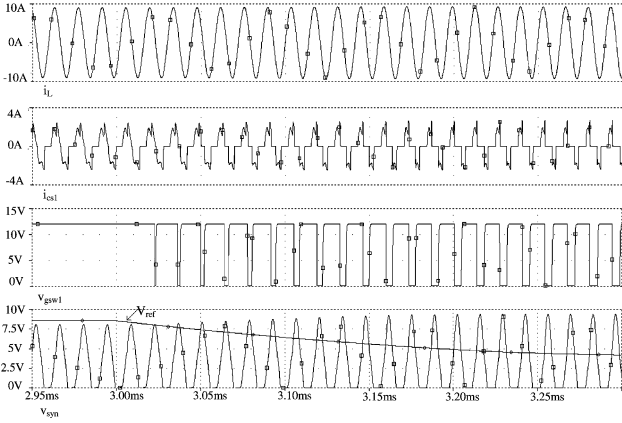


Fig. 10. Simulation waveforms of push-pull converter with switched detuning capacitors.

$V_{dc}$ . In other words, the regulation of  $V_{ref}$  can be based on the variation of  $V_{dc}$  (the difference between the actual value and the expected value of  $V_{dc}$ ). Even a simple proportional-integral-derivative (PID) controller, if properly designed, would be able to maintain the average value of  $V_{dc}$  at the expected level with slight fluctuations.

## V. SIMULATION AND EXPERIMENTAL RESULTS

PSpice simulations have been undertaken to analyze the proposed frequency control method. Fig. 10 shows the simulation waveforms of  $i_L$  (primary track current),  $i_{cs1}$ ,  $v_{gsw1}$ ,  $v_{syn}$ , and  $V_{ref}$ . It can be seen that the resonant voltage signal  $v_{syn}$  is compared with the reference voltage  $V_{ref}$  to generate the gate control signal  $v_{gsw1}$ . The WP supply operates under the minimum loading condition in the initial stage (0–3 ms). Both detuning switches are fully on (100% duty cycle), because the reference voltage  $V_{ref}$  is higher than the amplitude of  $v_{syn}$  ( $-v_{syn}$ ). When the load condition changes from the minimum to maximum value (load resistance changes from 10 k $\Omega$  to 33  $\Omega$  in the simulation) at 3 ms, the reference voltage  $V_{ref}$  starts dropping to reduce the duty cycle of the detuning switches and increasing the operating frequency. The simulated current ( $i_{cs1}$ ) is consistent with analytical predictions shown in Fig. 9.

A circuit capable of supplying 12 W has been built and tested. The primary and secondary coils were planar air core loops with an air gap of 4.5 cm. The main parameters of the primary resonant tank includes the primary coil inductance  $L_p = 12.2$   $\mu$ H, fixed tuning capacitor  $C = 220$  nF, and two switched capacitor  $C_{s1} = C_{s2} = 147$  nF. The secondary side self-inductance of pick-up coil was  $L_s = 5.4$   $\mu$ H, with resonant capacitor  $C_s = 835$  nF. The output dc voltage supplied to the load was

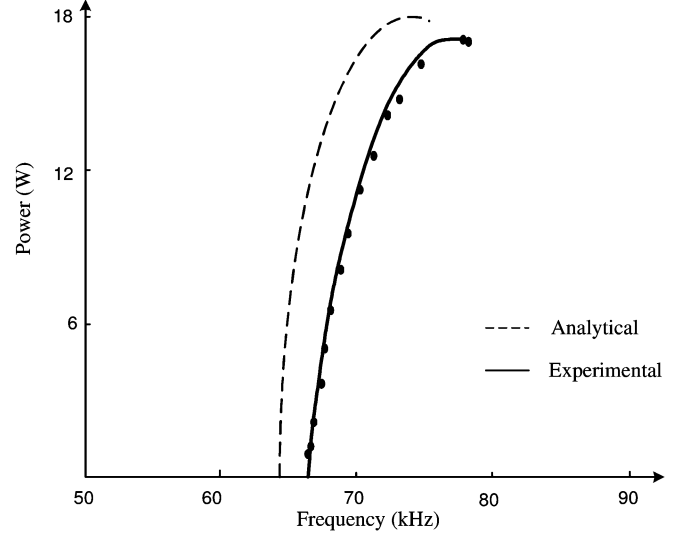


Fig. 11. Practical results of output power with component errors and ideal analytical results.

12 V. The power delivered was controlled within the range of 0–12 W.

In the experiments, the circuit operated in the left half range from  $f_1$  to  $f_0$ . Experimental results of the output power are shown in Fig. 11. As a comparison, an analytical curve based on ideal component parameters is also plotted in Fig. 11.

Although the shapes of experimental and analytical curve are in good agreement, the experimental curve deviates by about 3 kHz along the frequency axis. This is caused by deviations in actual component values from manufacturer's nominal values. For example, experimental results determined that the full tuning frequency was at 78.5 kHz which is almost 3.5 kHz higher than the analyzed full tuning frequency, 75 kHz. This result demonstrates a valuable attribute of this method in regulating load power effectively whilst compensating for a variety of other circuit parameter variations.

Fig. 12 shows the measured waveforms of the gate control signals for the main switch  $S_1$  (channel 1), gate control signal  $v_{gsw1}$  for detuning switch  $S_{w1}$  (channel 2), the synchronized signal of primary resonant voltage  $v_{syn1}$  (channel 3), and the feedback reference voltage  $V_{ref}$  (channel 4). It can be seen that the on-off commutation of the main switch  $S_1$  occurs at the zero crossing of the resonant voltage signal  $v_{syn1}$ , resulting in a constant duty cycle of 50% and full zero voltage switching. The detuning switch  $S_{w1}$  is switched on when the synchronized signal  $v_{syn1}$  is less than the reference voltage  $V_{ref}$  of 3.07 V, causing a duty cycle of 76.7%. The resonant frequency in this situation is 68.5 kHz, and only about 2.6 W is transferred to the load. The

$$P = I_{dc}V_{dc} = \frac{k\pi\hat{V}_{oc}^2}{4\sqrt{2}} \sqrt{\left(\frac{1}{L_s \cdot f(V_{ref})}\right) - \left[\frac{k\pi}{2\sqrt{2}} \left(C_t \cdot f(V_{ref}) - \frac{1}{L_s \cdot f(V_{ref})}\right)\right]}. \quad (15)$$

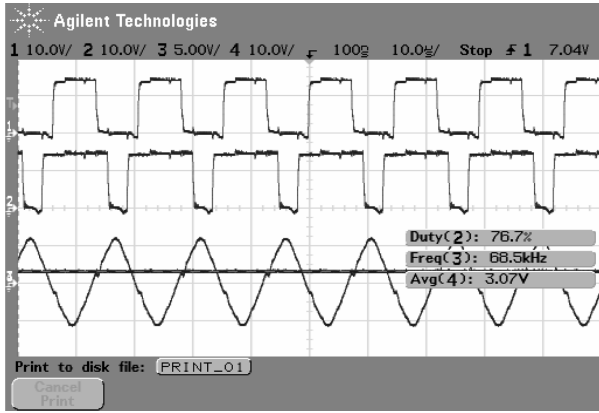


Fig. 12. Experimental waveforms: gate control signals for switch  $S_1$  and  $S_{w1}$  (Channel 1 and 2), resonant voltage signal  $v_{syn1}$  (Channel 3), and feedback reference voltage  $V_{ref}$  (Channel 4),  $P = 2.6$  W.

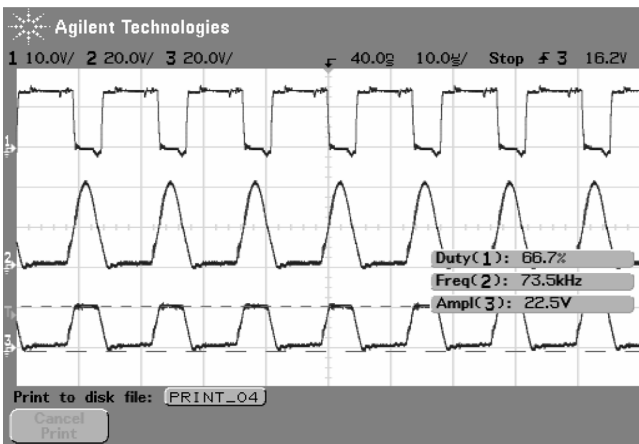


Fig. 13. Experimental waveforms: gate control signal for switch  $S_{w1}$  (Channel 1), voltage across the main switch  $S_1$  (Channel 2) and voltage across detuning capacitor  $C_{s1}$  (Channel 3),  $P = 14$  W.

waveforms shown in Fig. 12 are in a good agreement with the analytical results shown in Fig. 10.

When the power demand is increased to 14 W, the feedback reference voltage automatically drops to 1.74 V. Thus, the duty cycle of the detuning switches is reduced so as to increase the primary operating frequency for approaching higher power transfer capability. Fig. 13 shows the waveforms of the gate control signal  $v_{gsw1}$  of the detuning switch  $S_{w1}$  (channel 1), voltage across the main switch  $S_1$  (channel 2), and the voltage across the switched capacitor  $C_{s1}$  (channel 3). It can be seen that the duty cycle of the detuning switch is reduced to 66.7% causing a higher operating frequency of 73.5 kHz. The voltage across the main switch  $S_1$  is equal to the resonant voltage ( $v_c$ ) of the converter when it is off. The voltage across the switched capacitor  $C_{s1}$  is the same as the voltage across the main switch  $S_1$  when the detuning switch  $S_{w1}$  is on. This is because  $C_{s1}$  is in fact connected to  $S_1$  in parallel. However, the voltage across  $C_{s1}$  is constant when the switch  $S_{w1}$  is turned off. At this time no charging current flows through the capacitor  $C_{s1}$ , which is disconnected from  $S_1$  by turning  $S_{w1}$  off.

## VI. CONCLUSION

This paper has demonstrated a power regulation method based on controlling the frequency of a primary WP supply. It can achieve regulation in the presence of variations of multiple circuit parameters prevalent in the application of powering implantable medical devices.

The relationship between power delivered and primary operating frequency has been derived. It was shown that a larger boost-up-factor  $k$  requires a smaller frequency variation range for the full range of power flow control. Also, the maximum power transfer capacity is proportional to the boost-up-factor. The phase control method of implementing a variable capacitive element performs well in controlling the operating frequency of the push-pull resonant converter while maintaining full soft switching conditions. Experimental results have shown that the power delivered to the load can be regulated effectively under a wide variety of load requirements and reasonable circuit parameter variations.

Experimental results have demonstrated a power efficiency of 80% when transferring 15 W over a 10-mm air gap. Heating at the secondary coil was well below the target limit of 2 °C. However, conduction of heat from the primary coil causes the implantable coil temperature to increase approximately 6 °C. This result identifies the need for better thermal management on the primary side.

## REFERENCES

- [1] H. Honda, K. Shiba, E. Shu, K. Koshiji, T. Murai, J. Yana, T. Masuzawa, E. Tatsumi, Y. Taenaka, and H. Takano, "Study on lithium-ion secondary battery for implantable artificial heart," in *Proc. 19th Annu. Int. Conf. IEEE Eng. Med. Biol. Soc.*, Oct. 1997, vol. 5, pp. 2315–2317.
- [2] R. S. Sanders and M. T. Lee, "Implantable pacemakers," *Proc. IEEE*, vol. 84, no. 3, pp. 480–486, Mar. 1996.
- [3] O. H. Frazier, N. A. Shah, T. J. Myers, K. D. Robertson, I. D. Gregoric, and R. Delgado, "Use of the flowmaker (Jarvik 2000) left ventricular assist device for destination therapy and bridging to transplantation," *Cardiology-Int. J. Cardiovasc. Med., Surgery Pathol.*, vol. 101, no. 1-3, pp. 111–116, 2004.
- [4] H. Maki, Y. Yonezawa, E. Harada, and I. Ninomiya, "An implantable telemetry system powered by a capacitor having high capacitance," in *Proc. 20th Annu. Int. Conf. IEEE Eng. Med. Biol. Soc.*, Oct. 1998, vol. 4, pp. 1943–1946.
- [5] A. S. Berson, "Magnetic control and powering of surgically implanted instrumentation," *IEEE Trans. Magn.*, vol. MAG-19, no. 5, pp. 2157–2161, Sep. 1983.
- [6] R. Puers and G. Vandevoorde, "Recent progress on transcutaneous energy transfer for total artificial heart systems," *Artif. Organs*, vol. 25, no. Issue 5, pp. 400–405, May 2001.
- [7] G. Wang, W. Liu, R. Bashirullah, M. Sivaprakasam, G. A. Kendir, Y. Ji, M. S. Humayun, and J. D. Weiland, "A closed loop transcutaneous power transfer system for implantable devices with enhanced stability," in *Proc. 2004 Int. Symp. Circuits Syst.*, May 2004, vol. 4, pp. IV:17–20.
- [8] G. B. Joung and B. H. Cho, "An energy transmission system for an artificial heart using leakage inductance compensation of transcutaneous transformer," *IEEE Trans. Power Electron.*, vol. 13, no. 6, pp. 1013–1022, Nov. 1998.
- [9] G. Wang, W. Liu, M. Sivaprakasam, and G. A. Kendir, "Design and analysis of an adaptive transcutaneous power telemetry for biomedical implants," *IEEE Trans. Circuits Syst. I, Reg. Papers*, vol. 52, no. 10, pp. 2109–2117, Oct. 2005.
- [10] A. Ghahary and B. H. Cho, "Design of a transcutaneous energy transmission system using a series resonant converter," in *Proc. 21st Annu. IEEE Power Electron. Specialists Conf.*, Jun. 1990, pp. 1–8.
- [11] C. M. Zierhofer and E. S. Hochmair, "Geometric approach for coupling enhancement of magnetically coupled coils," *IEEE Trans. Biomed. Eng.*, vol. 43, no. 7, pp. 708–714, Jul. 1996.

- [12] P. Si, A. P. Hu, D. Budgett, S. Malpas, J. Yang, and J. Gao, "Stabilizing the operating frequency of a resonant converter for wireless power transfer to implantable biomedical sensors," in *Proc. 1st Int. Conf. Sensing Technol.*, New Zealand, Palmerston North, 2005, pp. 477–482.
- [13] A. P. Hu, "Selected Resonant Converters for IPT Power Supplies," Ph.D. dissertation, Dept. Elect. Comp. Eng., Univ. Auckland, Auckland, New Zealand, 2001.
- [14] P. Si and A. P. Hu, "Analyses of dc inductance used in icpt power pick-ups for maximum power transfer," in *Proc. IEEE/PES Transmission Distribution Conf. Exhibition 2005: Asia and Pacific*, Aug. 2005, pp. 1–6.
- [15] P. Si, A. P. Hu, J. W. Hsu, M. Chiang, Y. Wang, S. Malpas, and D. Budgett, "Wireless power supply for implantable biomedical device based on primary input voltage regulation," in *Proc. 2nd IEEE Conf. Industrial Electron. Appl.*, May 2007, pp. 235–239.
- [16] J. C. Schuder, "Powering an artificial heart: Birth of the inductively coupled-radio frequency system in 1960," in *Artificial Organs, International Society for Artificial Organs 2002*, Nov. 2002, vol. 26, pp. 909–915.
- [17] A. W. Green and J. T. Boys, "10 kHz inductively coupled power transfer-concept and control," in *Proc. 5th Int. Conf. Power Electron. Variable-Speed Drives 1994.*, Oct. 1994, pp. 694–699.

**Ping Si** (M'04) received the B.S. degree in electrical engineering from Xian JiaoTong University, Xi'an, China, in 1998, the Graduate Diploma in computer science from the University of Auckland, New Zealand, in 2002, where he is currently pursuing the Ph.D. degree in the Department of Electrical and Computer Engineering.

From 1998 to 1999 he worked as an engineer at the Northwest Electrical Power Testing Research Institute, China. His research is to develop high-quality wireless power supplies for implantable biomedical devices.

**Patrick Aiguo Hu** (M'98–SM'07) received the B.E. and M.E. degrees from Xian JiaoTong University, Xi'an, China, in 1985 and 1988, respectively, and the Ph.D. degree from the University of Auckland, Auckland, New Zealand, in 2001.

Prior to that, he worked as a Lecturer, an Electrical Engineer, Group Leader, and later the Director of a technical section in China. He holds a few patents in microcomputer control and inductive power transfer technologies, and co-authored a book on electrical machines. He is currently a Senior Lecturer in the Department of Electrical and Electronic Engineering, the University of Auckland. His research interests include wireless power transfer, power converters, and application of power electronics in power systems.

Dr. Hu is a co-chair of the New Zealand IEEE Power Engineering and Power Electronics Joint Society. He received the University of Auckland Ph.D. scholarship, the Asian 2000 Foundation Scholarship for a four-month study visit to the National University of Singapore, and an industrial scholarship from Wampfler AG, Germany.

**Simon Malpas** received the Ph.D. degree from Otago University, Otago, Japan, in 1990.

He worked as a Postdoctoral Research Fellow in Japan, the U.K., and Australia from 1990–1996 in the area of blood pressure control with particular reference to the role of the sympathetic nervous system. He is currently an Associate Professor in the Department of Physiology and the Bioengineering Institute, University of Auckland, Auckland, New Zealand. He is head of the Circulatory Control Laboratory whose research focus is on the role of sympathetic activity in the development of hypertension.

**David Budgett** received the Ph.D. degree in biomedical engineering from Imperial College London, London, U.K., in 1995.

He has held academic positions at the University of Sussex and the University of Auckland with research interests in medical devices. He leads a team developing implantable telemetry devices in the Bioengineering Institute, University of Auckland, Auckland, New Zealand.